

Exploring the Electronic Potential of Effective Tight–Binding Hamiltonians

Graziâni Candiotto^a

^aInstituto de Física, Universidade Federal do Rio de Janeiro, Rio de Janeiro, 21941-972, RJ, Brazil

Abstract

The linear combination of atomic orbitals (LCAO) is a standard method for studying solids and molecules, it is also known as the tight–binding (TB) method. In most of the implementations only the basis set and the coupling constants are provided, without the explicit definition of kinetic and potential energy operators. The tight–binding scheme is, nonetheless, capable of providing an accurate description of properties such as the electronic bands and elastic constants for many materials. However, for some applications, the knowledge of the underlying electronic potential associated with the tight–binding hamiltonian might be important to guarantee that the actual physics is preserved by the semiempirical scheme. In this work the electronic potentials that arise from the use of tight–binding effective hamiltonians it is explored. The formalism is applied to the extended Hückel tight–binding (EHTB) hamiltonian, which is a two–center Slater–Koster approach that makes explicit use of the overlap matrix.

Keywords: Effective potential, Tight–binding

1. INTRODUCTION

The linear combination of atomic orbitals (LCAO), also known as tight–binding (TB) method, is largely used for describing the transport properties in condensed matter,[1–5] for studying the electronic structure of complex solids[6–8] and large molecular systems,[9–11] for performing molecular dynamics,[12] among other applications. Several TB prescriptions have been developed since the original proposal of Slater and Koster.[13] Noteworthy, the tight–binding density functional theory (TB–DFT) method has been used as an efficient alternative for the calculation of the electronic structure and for molecular dynamics simulations of large systems.[14–17] The TB or LCAO schemes consist of making a linear combination of atomic orbitals, localized on the atomic positions, as a means for developing the bonding interactions in terms of site–centered orbitals. Due to its simplicity and versatility, much knowledge has been gained through the use of tight–binding methods. For instance, the method is capable of describing accurately the total energy of solids and molecules, the energy differences caused by small structure deformations and the associated phonon spectra.[7] It can also reproduced the equations of state and defect energies,[8, 18] among other structural properties.

To best describe the properties of the system a set of TB parameters must be tuned so that the calculations fit some reference data set, which may either be obtained from higher level theory or gathered from experiments. If well parametrized, the method can accurately reproduce *ab–initio* calculations for a variety of materials – including transition and noble metals,[18, 19] semiconductors,[7] and molecules [3] – but with a much lower computational cost. Therefore complex problems and materials can be studied for the first time.

However, for some applications, it might be necessary to dis-

cern the actual couplings that are implied by the tight–binding parameters, because the effective TB hamiltonian aims at describing only the total energy of the state, disregarding whether it is kinetic or due to a potential. The knowledge of the underlying electronic potential associated with the tight–binding method is important to guarantee that the actual physics is preserved by the semiempirical scheme, since several parameter sets can frequently fit the data. In this work the electronic potentials that result from the use of tight–binding effective hamiltonians is explored. The formalism is applied to the extended Hückel tight–binding (EHTB) hamiltonian, which has been widely used by physicists, chemists and materials scientist to describe the electronic structure and properties of molecules and solids. The EHTB method corresponds to a two–center Slater–Koster approach that makes explicit use of the overlap matrix, which brings to the model information about disorder, molecular shape, molecular arrangement, as well introduce interactions between atomic orbitals in a molecule or solid.

The EHTB method is in essence a two–center Slater–Koster formulation of tight–binding with a nonorthogonal basis. According to the extended Hückel prescription, the elements of the hamiltonian matrix are written as a linear function of the overlap (or adjacency) matrix \mathbf{S} . Thus, for a given basis set

$$\begin{aligned}\langle i|\mathbf{H}|j\rangle &= \xi_{ij}\langle i|j\rangle, \\ H_{ij} &= \xi_{ij}S_{ij},\end{aligned}\quad (1)$$

where $\{|i\rangle\}$ is some generic local basis set $\chi_i(\mathbf{r}) = \langle \mathbf{r}|i\rangle$. ξ_{ij} is commonly written as

$$\xi_{ij} = K_{ij}\left(\frac{E_i + E_j}{2}\right),\quad (2)$$

where K_{ij} is a coupling parameter, which is usually set to 1.75 if $i \neq j$, or 1 if $i = j$. The diagonal elements of \mathbf{H} , the

E_{ij} parameters, may be chosen to represent the valence ionization potentials of the atomic species, or the on-site energies associated with the localized basis set. That way a small set of semi-empirical parameters suffice to build up the hamiltonian, which renders the EHTB method a clear physical interpretation, with a reduced number of semiempirical parameters (as compared to the SK method) and good transferability, because it makes explicitly use of the overlap matrix. Thereby, the method accounts approximately for effects produced by geometrical and chemical bond variations.[11] The EH hamiltonian can be mapped onto the traditional TB Hamiltonian form,

$$\widehat{H}_{tb} = \sum_i \epsilon_i \widehat{a}_i^\dagger \widehat{a}_i - \sum_{i \neq j} t_{ij} \widehat{a}_i^\dagger \widehat{a}_j + c.c., \quad (3)$$

by choosing the parameters

$$\begin{aligned} \epsilon_i &= K_{ii} E_i, \\ -t_{ij} &= K_{ij} \left(\frac{E_i + E_j}{2} \right) S_{ij}. \end{aligned} \quad (4)$$

The diagonal elements of \mathbf{H} are called Coulomb Integrals; they represent the combined kinetic and potential energies of an electron described by the orbital $\chi_i(\mathbf{r})$, experiencing the electrostatic interactions with all the other electrons and all the positive nuclei. The off-diagonal elements are called Resonance (or Bond) Integrals.[20] In addition to the Slater-type orbitals originally proposed by Hoffmann,[20] other simple algebraic forms may be used for basis set: for instance, Gaussian or harmonic oscillator basis functions. The EHT, when compared to the traditional SK tight-binding method, provides good accuracy while presenting several important advantages:[4, 7] i) a considerable reduction in the number of parameters to be fitted, ii) natural scaling laws for the coupling parameters and, iii) an improved transferability of the parameters.

In the remainder of the paper it is described, in section 2, the formalism used to obtain the effective electronic potential associated with the Extended Hückel tight-binding (EHTB) hamiltonian is presented and applied in the calculation it for several prototypical molecular systems. In section 3 the method is applied to a model for two-dimensional quantum dot arrays and in section 4 the main conclusions of this study are presented.

2. Electronic Tight-Binding Potential

The tight-binding hamiltonian is not constructed from the kinetic (\widehat{T}) or Coulomb potential (\widehat{V}) operators but it is, otherwise, directly determined by the basis set functions $\chi_i(\mathbf{r})$, or simply built up from a set of appropriate coupling parameters. As a result, several parameter sets can frequently fit the reference set, with different electronic potentials associated to them. It is, therefore, desirable to know that the underlying physics is preserved by the parametrization scheme. In this section it is presented a procedure to determine the effective electronic potential that results from the use of a tight-binding hamiltonian.

For an operator \widehat{O} , written in terms of a nonorthogonal basis set, one has

$$\begin{aligned} O(\mathbf{r}, \mathbf{r}') &= \langle \mathbf{r} | \widehat{O} | \mathbf{r}' \rangle, \\ &= \langle \mathbf{r} | \left[\sum_{n,i} |n\rangle S_{ni}^{-1} \langle i| \right] \widehat{O} \left[\sum_{j,m} |j\rangle S_{jm}^{-1} \langle m| \right] | \mathbf{r}' \rangle, \\ &= \sum_{\substack{n,m \\ i,j}} \langle \mathbf{r} | n \rangle S_{ni}^{-1} \langle i | \widehat{O} | j \rangle S_{jm}^{-1} \langle m | \mathbf{r}' \rangle, \\ &= \sum_{\substack{n,m \\ i,j}} \chi_n(\mathbf{r}) S_{ni}^{-1} O_{ij} S_{jm}^{-1} \chi_m(\mathbf{r}'), \end{aligned} \quad (5)$$

where the sums are carried over all basis states. By defining $\widehat{\mathbf{O}} = \mathbf{S}^{-1} \mathbf{O} \mathbf{S}^{-1}$ it is avoided the trouble of dealing with the nonorthogonality of the basis, thus

$$O(\mathbf{r}, \mathbf{r}') = \sum_{n,m} \chi_n(\mathbf{r}) \widehat{O}_{nm} \chi_m^*(\mathbf{r}'). \quad (6)$$

The operator $O(\mathbf{r}, \mathbf{r}')$ accounts for the interference of wavefunctions $\chi_n(\mathbf{r})$ and $\chi_m^*(\mathbf{r}')$. The operator \widehat{O} can be formally written in the $|n\rangle$ representation as

$$\widehat{O} = \sum_{n,m} |n\rangle \widehat{O} \langle m|, \quad (7)$$

as well as

$$\widehat{O} = \int \int |\mathbf{r}\rangle O(\mathbf{r}, \mathbf{r}') \langle \mathbf{r}'| d\mathbf{r} d\mathbf{r}', \quad (8)$$

in the representation of the coordinates. However, if the single particle operator \widehat{O} happens to be a local function of \widehat{r} , *i.e.*, $\widehat{O} = f(\widehat{r})$ (like the Coulomb or the harmonic oscillator potentials), then \widehat{O} must be diagonal in the coordinates

$$\begin{aligned} \widehat{O} &= \int \int |\mathbf{r}\rangle O(\mathbf{r}, \mathbf{r}') \delta(\mathbf{r} - \mathbf{r}') \langle \mathbf{r}'| d\mathbf{r} d\mathbf{r}', \\ &= \int |\mathbf{r}\rangle f(\mathbf{r}) \langle \mathbf{r}| d\mathbf{r}. \end{aligned} \quad (9)$$

So far it has been assumed a complete basis set $|n\rangle$, but if this is not the case, it is possible to write

$$\begin{aligned} \widehat{O} &\approx \widehat{O}_N \equiv \sum_{n,m}^N |n\rangle \widehat{O}_{nm} \langle m|, \\ &\equiv \sum_k^N \widehat{O}^{(k)}, \end{aligned} \quad (10)$$

where N is the truncation order and

$$\begin{aligned} \widehat{O}^{(k)} &= \sum_{n,m}^k |n\rangle \widehat{O}_{nm} \left(\frac{\delta_{nk} + \delta_{mk}}{1 + \delta_{nk} \delta_{mk}} \right) \langle m|, \\ &= \sum_{n,m}^k |n\rangle \widehat{O}_{nm} \Delta_{nm}^{(k)} \langle m|, \end{aligned} \quad (11)$$

as depicted below

$$\widehat{O} = \begin{pmatrix} \widetilde{O}_{11} & \widetilde{O}_{12} & \widetilde{O}_{13} & \cdots \\ \widetilde{O}_{21} & \widetilde{O}_{22} & \widetilde{O}_{23} & \cdots \\ \widetilde{O}_{31} & \widetilde{O}_{32} & \widetilde{O}_{33} & \cdots \\ \vdots & \vdots & \vdots & \ddots \end{pmatrix}. \quad (12)$$

In Eq. (11) the numerator selects the k -th column, and the denominator normalizes the factor 2 that appears for diagonal elements, $i = j = k$. It will be shown in section 3 that the truncation of this operator affects the nonlocality of the potential. By using the TB hamiltonian one has no knowledge of the kinetic and potential energy components of the particles, except for the fact that, in principle, the eigenstates diagonalize some effective hamiltonian $H_\chi = T_\chi + V_\chi$. Only H is known in the representation of the truncated basis set functions $\{\chi_i(\mathbf{r})\}$. However, it is possible to apply the Kohn–Sham ansatz [21] and assume that the kinetic energy is equal to the kinetic energy of a system of a non-interacting particles. By writing the kinetic energy (in atomic units) as

$$T_{ij} = \langle i | \nabla^2 | j \rangle, \quad (13)$$

so it is possible to introduce an effective electric potential \mathbf{V} , which is defined as

$$\begin{aligned} V_{ij} &= H_{ij} - T_{ij}, \\ &= \xi_{ij} S_{ij} - T_{ij}. \end{aligned} \quad (14)$$

Thus, it becomes possible to map the TB hamiltonian onto a dynamic system, where it is possible to calculate the kinetic energy and the potential \mathbf{V} .

Thus far, \mathbf{T} and \mathbf{V} were determined in the representation of basis $\{|n\rangle\}$, however $V(\mathbf{r})$ is more amenable to interpretation than V_{ij} . Then, rewrite the potential in the representation of the coordinates as

$$V(\mathbf{r}, \mathbf{r}') = \sum_{n,m} \chi_n(\mathbf{r}) \widetilde{V}_{nm} \chi_m^*(\mathbf{r}'). \quad (15)$$

Although $V(\mathbf{r}, \mathbf{r}')$ should be local for an independent particle, that is not the case due to the approximations undertaken, which are the basis space truncation and the use of the KS ansatz. Though it is not possible to assume that $V(\mathbf{r}, \mathbf{r}')$ is diagonal, one can expect that this is a reasonable approximation, since the local density approximation (LDA)[21, 22] is known to work well for systems without strong correlations. Therefore it is defined

$$V_{eff}(\mathbf{r}) = V(\mathbf{r}, \mathbf{r}). \quad (16)$$

This local form will be used in the following to obtain the effective potential of the EHTB method.

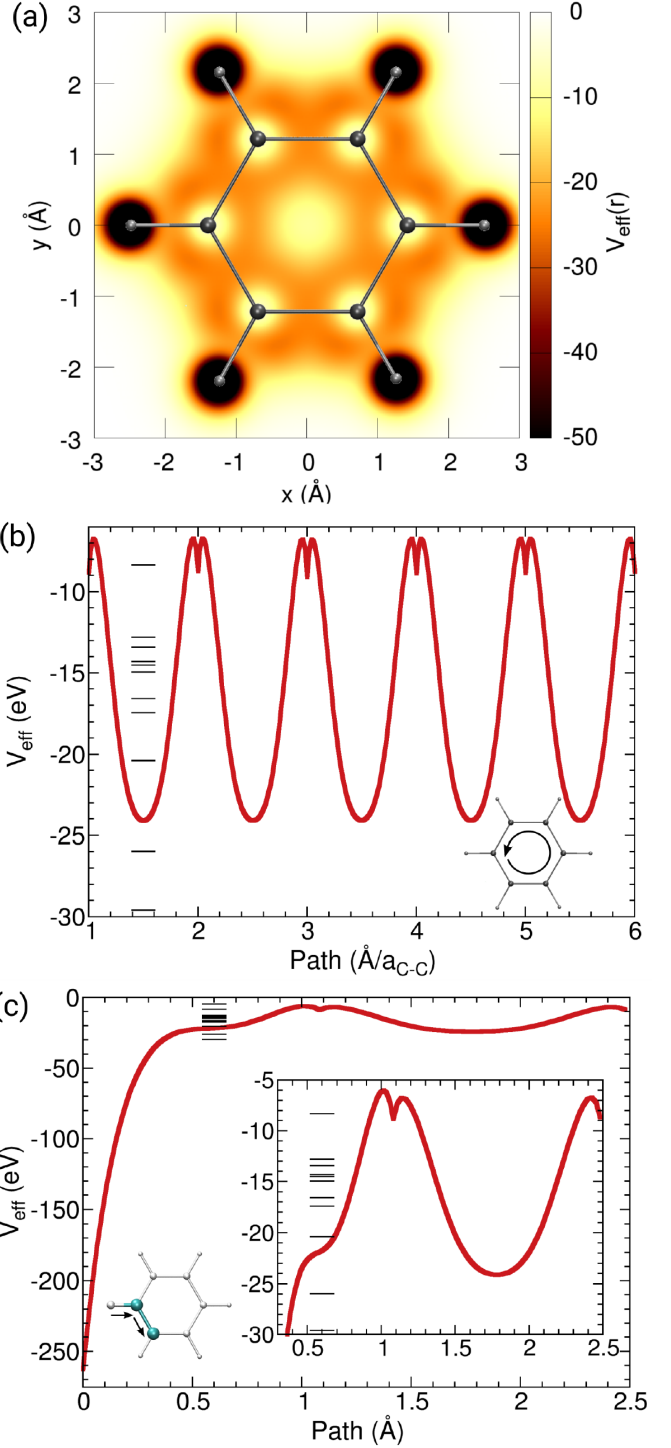


Figure 1: EHT electronic potential $V_{eff}(\mathbf{r})$ for the benzene molecule: a) surface map of $V_{eff}(\mathbf{r})$; b) $V_{eff}(\mathbf{r})$ along the contour of carbon cycle, the distance along the path is measured in units of the C–C. The horizontal lines show the energies of the molecular orbitals (eigenstates of the EHT hamiltonian) up to the HOMO level; c) the potential along the H–C–C path, with distance measured in Å.

2.1. The Electronic Potential of the Extended Hückel Tight–Binding Method

Having defined the effective electronic potential operator, the EHTB $V_{eff}(\mathbf{r})$ was calculated for some prototypical molecules.

Recalling that the functional form of the electronic potential shall be determined by both the tight-binding parameters as well as the basis set. The basis set functions generally employed to describe chemical species are the Slater-type orbitals (STO), defined as

$$\chi_{nml}(\mathbf{r}) = r^{(n-1)} e^{-\zeta r} Y_l^m(\theta, \phi). \quad (17)$$

For the STO's, ζ is a semiempirical parameter related to the effective charge of the ion, n is the main quantum number and the $Y_l^m(\theta, \phi)$ are spherical harmonics. The radial part of the wavefunctions (Eq. 17) characterize the Slater-type orbitals. To simplify the notation in the following equations, the indices n, l, m , and ζ , are combined into one global index N , and write $|N\rangle = |nlm; \zeta\rangle$.

The kinetic energy matrix elements between two STOs centered at \mathbf{R}_A and \mathbf{R}_B can be written as a sum of overlap elements (see ref. [23]),

$$\begin{aligned} T_{N'N}^N &= -\frac{1}{2} \langle n'l'm'; \zeta' | \nabla^2 | nlm; \zeta \rangle, \\ &= -\frac{1}{2} \left\{ [n(n-1) - l(l+1)] S_{n'l'm'}^{(n-2)lm} \right. \\ &\quad \left. - 2n\zeta S_{n'l'm'}^{(n-1)lm} + \zeta^2 S_{N'}^N \right\}. \end{aligned} \quad (18)$$

In the calculations that follow, standard Hoffmann parameters are used for the H, C, N, O and S atoms,[24] unless explicitly noted otherwise. The basis set includes the $3s$ and $3p$ atomic orbitals for S atoms, $2s$ and $2p$ atomic orbitals for C, N and O atoms, and the $1s$ atomic orbital for H atoms.

Starting by analysing the Extended Hückel electronic potential of the benzene molecule, as presented in Figure 1, where the top image shows a surface map of $V_{eff}(\mathbf{r})$; graphs b) and c) show the EHTB potential along different paths in the molecular structure, as indicated by the insets. This figure evinces the general features of the EHTB potential produced by the Slater-type orbitals. Along the carbon ring (Figure 1b), the potential minima is located in the bond region – not on the site of the C atoms – because only the valence states ($2s$ and $2p$) are used to describe these atoms. The former orbitals are mostly involved with the formation of bonds, via the resonance (off-diagonal) terms of the extended Hückel hamiltonian. The effect it produces on the EHTB potential is analogous to the effect produced by the use of pseudo-potentials in first-principles calculations, [25] which are employed to avoid the ionic potential at the core region. The potential is a lot deeper, however, on the site of the H atom (Figure 1c), since it is the result of only the $1s$ orbital. The energies of the molecular orbitals (MO), up to the HOMO level, as obtained by solving the EHTB eigenvalue equation for the C_6H_6 molecule, are depicted by horizontal bars alongside $V_{eff}(\mathbf{r})$. Despite the deep quantum wells on the hydrogen sites the energies of the MOs are comparable to the bonding potentials of the carbon ring.

To analyze the effect produced by different atoms it was calculated $V_{eff}(\mathbf{r})$ for four pentagonal molecules of distinct compositions, namely: thiophene (SC_4H_4), pyrrole (NC_4H_5), furan (OC_4H_4) and cyclopentadienyl (C_5H_5). Their EHTB potentials

are shown in Figure 2, color coded as: SC_4H_4 (orange), NC_4H_5 (blue), OC_4H_4 (red) and C_5H_5 (black). Along the molecular ring the $V_{eff}(\mathbf{r})$ shows the same characteristics as in the benzene molecule (Figure 1), except on the position of the heteroatom. In this case, the effective potential is deeper for the C–O bond, followed by C–N, C–C and C–S, reflecting the different electronegativity of the elements (3.44 for O, 3.04 for N, 2.55 for C and 2.58 for S).

A more demanding calculation was performed for the 2-(2'-hydroxyphenyl)benzothiazole (HBT) molecule, shown in Figure 3. In this case, the standard EHTB parameters did not yield a good description of the molecule's HOMO–LUMO gap, neither of its dipole moment. Thus, in order to obtain parameters that are more consistent with the HBT molecule, a functional density theory (DFT) was used to obtain the dipole moment and the HOMO–LUMO energy gap as references. First the HBT molecule was relaxed to ground state geometry using a genetic-algorithm scheme[26]. In DFT calculations, the hybrid functional Becke three-parameter Lee–Yang–Parr (B3LYP)[27, 28] was used along with a split-valence double-zeta polarized Gaussian type orbital basis, 6–31G (d, p)[29]. For the sake of comparison with the *ab-initio* theory it is presented the dipole moments, 1.99 Debye and 2.02 Debye for the DFT and EHT methods, respectively, and the HOMO–LUMO gap of 4.14 eV for DFT and 4.22 eV for EHT. Figure 3 presents the surface map of $V_{eff}(\mathbf{r})$, with two arrows superposed to it, which represent the dipole moment vectors obtained by the DFT (red) and EHT (blue) calculations. Both the orientation and size of the dipole moments show excellent agreement. It is interesting to notice also that the effective potential exhibits a strong gradient along the same direction as the electronic dipole moments, that is, deeper at the OH enol group and shallower on the S atom of the thiazole heterocycle. That potential gradient gives rise to electron concentration on the OH enol group and charge depletion around the S atom.

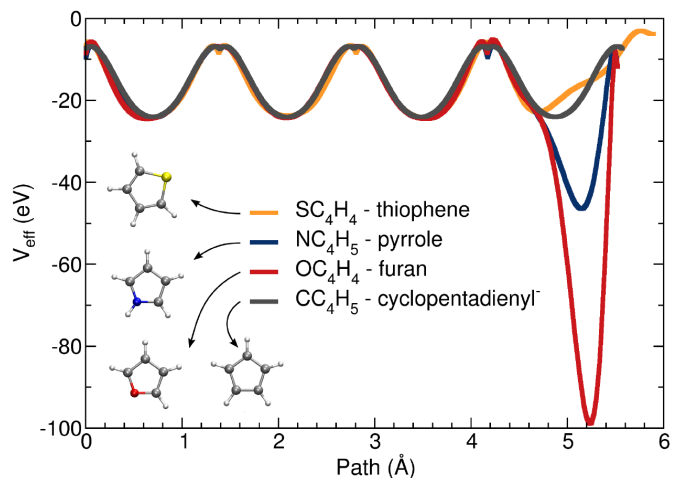


Figure 2: EHT electronic potential $V_{eff}(\mathbf{r})$ for the pentagon-shaped molecules: thiophene (SC_4H_4 , orange), pyrrole (NC_4H_5 , blue), furan (OC_4H_4 , red) and cyclopentadienyl (C_5H_5 , black). $V_{eff}(\mathbf{r})$ along the contour of the ring, with distance measured in Å.

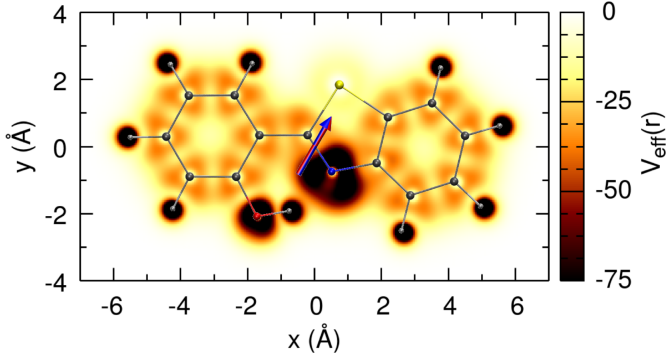


Figure 3: Surface map of the EHT electronic potential $V_{eff}(\mathbf{r})$ for the 2-(2'-hydroxyphenyl)benzothiazole (HBT) molecule (geometry superposed). The arrows describe the electric dipole moments, as calculated with DFT (1.99 Debye, red) and EHT (2.02 Debye, blue).

3. QUANTUM DOT ARRAYS

The linear combination of harmonic functions associated to localized parabolic potentials can describe charge and energy transport in quantum dot arrays, [30, 31] artificial molecules and mesoscopic devices, [32, 33, 33] organic and supramolecular structures, [34–36] and photonic crystals [37]. In this section it is applied the effective potential method to a system comprised of localized parabolic quantum wells.

Firstly it is analysed a model of two coupled parabolic wells, as shown in Figure 4, with the goal of comparing the obtained $V_{eff}(\mathbf{r})$ with the actual potential profile. Assuming that the electronic structure of the harmonic dimer is given by the EHTB model, calculated on the basis of the harmonic oscillator eigenstates

$$\chi_n(x) = \frac{1}{\sqrt{2^n n!}} \left(\frac{m\omega}{\pi} \right)^{1/4} \exp\left(-\frac{m\omega x^2}{2\hbar}\right) H_n(\alpha x), \quad (19)$$

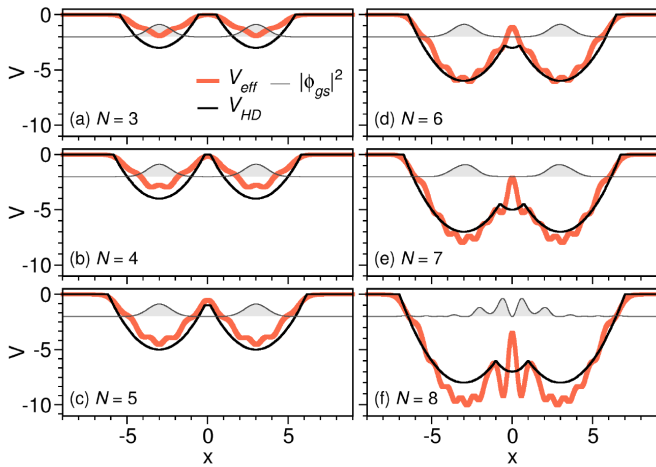


Figure 4: Effective potential $V_{eff}(x)$, harmonic dimer potential $V_{HD}(x)$ and ground state probability density $|\phi_{gs}(x)|^2$ (grey shade), for various basis set sizes: from $N = 3$ to $N = 8$, in (a) to (f), respectively. $|\phi_{gs}(x)|^2$ is scaled by two and arbitrarily shifted for easier visualization).

where H_n is the Hermite polynomial of argument $\alpha = \sqrt{m\omega/\hbar}$ and n order, associated with the energy eigenvalue

$$E_n = \hbar\omega \left(n + \frac{1}{2} \right). \quad (20)$$

To assure that the energy of the bound states are negative, it is shifted the Extended Hückel hamiltonian by the value $E_{shift} = \hbar\omega(N + 1/2)$, as follows

$$H_{ij} = \left[K_{ij} \left(\frac{E_i + E_j}{2} \right) - E_{shift} \right] S_{ij}, \quad (21)$$

where the integer N designates the number of bound states. The elements S_{ij} of the overlap matrix can be calculated analytically for the orbitals (Eq. 19). In Figure 4 we show the effective potential V_{eff} (red curve) and the actual potential of the harmonic dimer (HD) V_{HD} (black line), for an increasing number of bound states: from $N = 3$ to $N = 8$. Notice that the intersection of the two parabolic wells gives rise to another parabolic well centered at the origin. We observe that V_{eff} and V_{HD} differ more significantly if the number of basis states is too few ($N < 5$) or too many ($N > 7$). In the former case there are not enough basis functions to describe the bound states whereas, in the later, the delocalized basis functions start to interfere. The probability density of the ground ($|\phi_{gs}(x)|^2$) is also shown, scaled by two and arbitrarily shifted for the sake of visualization. These eigenstates are solutions of the EHTB eigenvalue equation $\mathbf{HC} = \mathbf{ESC}$, obtained for the hamiltonian (Eq. 21) in the nonorthogonal basis set $\{\chi_n\}$, where \mathbf{C} is the vector associated to $\phi(x) = \sum_n C_n \chi_n(x)$.

Although $V_{eff}(\mathbf{r})$ is defined as a local potential by Eq. 16, the effective potential is actually nonlocal, as given by Eq. 15. For the nonlocal potential, the energy term $U(x) = V(x)\phi(x)$ in the Schrödinger equation is replaced by

$$U(x) = \int V(x, x') \psi(x') dx' \quad (22)$$

where the kernel $V(x, x')$ contains the nonlocal dependence. So far the local (diagonal) part of the effective potential has been shown, but in Figure 5 it is showed the behavior of the nonlocal effective potential for the harmonic dimer, for basis sizes $N = 3, 5, 7$ and 9 . From the physical viewpoint, nonlocal potentials can alter the solution of a local double-well potential by producing wavefunctions with more nodes than those of the local potential, [38] by changing the size of the local barrier and, consequently, the tunneling dynamics. [39] These effects can give rise to anomalous diffusion [40] and, therefore, affect the calculated transport properties of the system. For the harmonic dimer presently considered (Figure 5) the nonlocality is of short range and does not couple the two wells until they start to merge, for $N \geq 8$, but if the coupling parameter increases the nonlocality of the effective potential is expected to increase.

At this moment the EHTB method it will be applied to calculate the effective potential for a two-dimensional array of quantum dots (2D-QD). For this application, a natural photosynthetic complex present in photosynthetic membrane of *Rhodospirillum rubrum* was chosen. The natural photosynthetic complex used in the calculations was taken from an

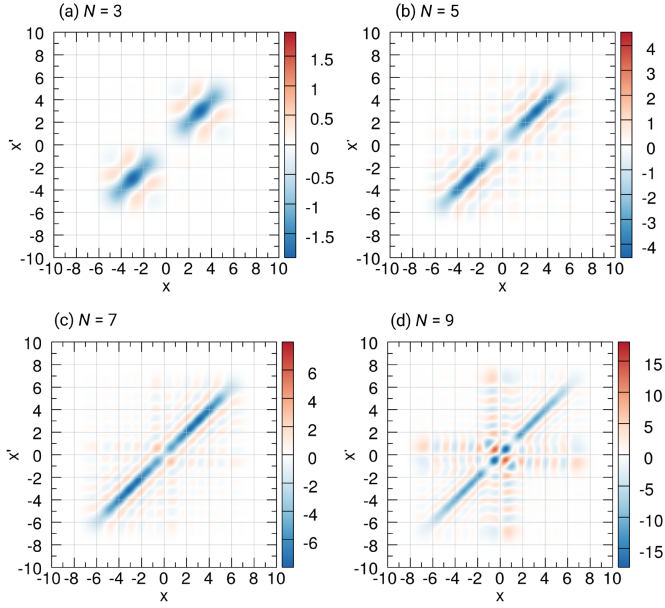


Figure 5: Potential operator in coordinates representation, $V(x, x')$ for $N = 3, 5, 7, 9$.

atomic force microscopy (AFM) image present in the ref. [36]. This supramolecular structure containing around 160 subunits. This system is basically characterized by two distinct subunits called light harvest complex I (LHC_I , large rings) and light harvest complex II (LHC_{II} , small rings). The subunit LHC_{II} is responsible for collecting (most of) the light that reaches the membrane, converting it into excitonic energy and transferring this energy to the LHC_I subunit where the reaction center is located, which is responsible for converting excitonic energy into chemical energy. On the other hand, the LHC_I subunit is responsible for collecting (part of) the light that reaches until the membrane, converting it into excitonic energy and transferring it to the reaction center, as well as receiving the excitonic energy originating from the LHC_{II} subunits. Thus, in the model each subunit (LHC_I and LHC_{II}) of the photosynthetic system will be modeled as a QD, where the electronic structure of subunits will be described by the EHTB calculated on the basis of the 2D harmonic oscillator

$$\chi_{n_x n_y}(x, y) = A_{n_x n_y} \exp\left[-\frac{m\omega}{2\hbar}(x^2 + y^2)\right] H_{n_x}(\alpha x) H_{n_y}(\alpha y), \quad (23)$$

being the argument $\alpha = \sqrt{m\omega/\hbar}$, while the energy eigenvalue are written as

$$E_{n_x n_y} = E_{n_x} + E_{n_y} = (n_x + n_y + 1) \hbar\omega, \quad (24)$$

where the normalization constant is

$$A_{n_x n_y} = \frac{1}{\sqrt{2^{(n_x+n_y)} n_x! n_y!}} \sqrt{\frac{m\omega}{\pi\hbar}}. \quad (25)$$

The kinetic energy matrix elements between two eigenstates given by Eq. 23 can be written as a sum of overlap elements

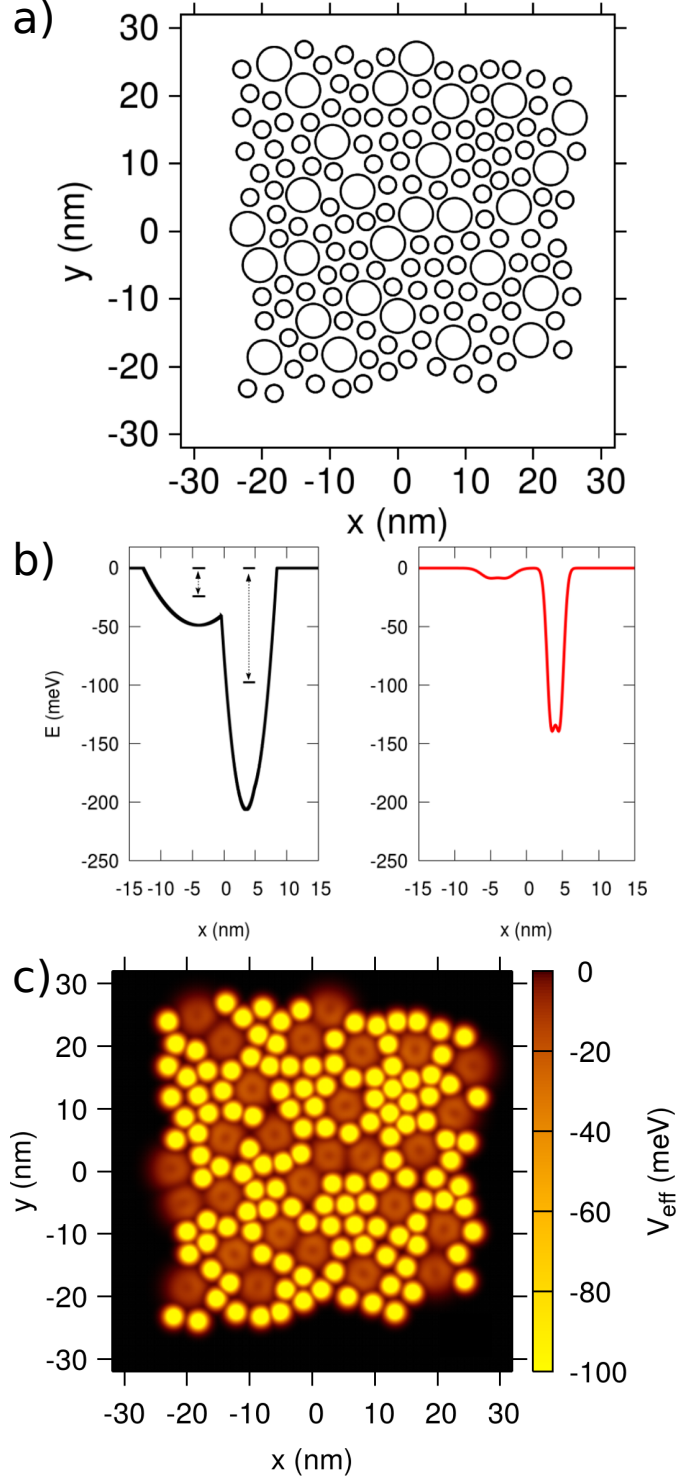


Figure 6: a) Two-dimensional array of quantum dots, where the large dots have a radius $R_1 = 2.5$ nm and the small ones $R_2 = 1.25$ nm. b) Left side, black curve: parabolic potentials and the characteristic energies ω_1 and ω_2 . Right side, red curve: the EHTB effective electronic potential, $V_{eff}(r)$. c) The EHTB effective electronic potential $V_{eff}(r)$ for the 2D-QD array.

as

$$\begin{aligned}
T_{n'_x n'_y}^{n_x n_y} = \frac{\hbar\omega}{4} \left\{ & 2(n'_x + n'_y + 1) S_{n'_x n'_y}^{n_x n_y} \right. \\
& - [n'_x (n'_x - 1)]^{1/2} S_{n'_x - 2, n'_y}^{n_x n_y} \\
& - [n'_y (n'_y - 1)]^{1/2} S_{n'_x, n'_y - 2}^{n_x n_y} \\
& - [(n'_x + 1)(n'_x + 2)]^{1/2} S_{n'_x + 2, n'_y}^{n_x n_y} \\
& \left. - [(n'_y + 1)(n'_y + 2)]^{1/2} S_{n'_x, n'_y + 2}^{n_x n_y} \right\}, \quad (26)
\end{aligned}$$

where ω is the characteristic frequency of the QD whose kinetic energy is calculated and \mathbf{S} is the overlap matrix between dot states.

The EHTB method was used to study the two-dimensional array of quantum dots shown in Figure 6a, this sketch of rings was taken from the AFM image of photosynthetic membrane of *Rhodospirillum photometricum* present in the ref. [36], where the large rings have a radius $R_{LHC_I} = 2.5$ nm and the small ones $R_{LHC_{II}} = 1.25$ nm. Defining the relation $R = \sqrt{2\hbar/(m\omega)}$ between the radius of the dot and the energy of the bound states, thereby the characteristic energy of the dots are $\omega_{LHC_I} = 24.4$ meV and $\omega_{LHC_{II}} = 97.5$ meV, as depicted at the left-hand side of Figure 6b, together with the parabolic potentials that generate the basis set $\chi_{n_x n_y}(\mathbf{r})$. On the right-hand side, the red curve describes the EHTB effective electronic potential, $V_{eff}(\mathbf{r})$, obtained for two neighboring QDs of different sizes and the truncated basis set $\{(n_x, n_y)\} = \{(00), (10), (01)\}$ which correspond to $\{s, p_x, p_y\}$ atomic orbitals. The two main differences between the parabolic potentials (left) and the effective potential (right) can be discerned as: the two QDs can be resolved by $V_{eff}(\mathbf{r})$ but not by the parabolic potentials and, besides that, the effective potential is shallower. The EHTB effective potential is, thus, calculated for the entire array with the result shown by the surface map in Figure 6c, which describes quite well the geometry of the 2D-QD array pictured in Figure 6a. Therefore, it is concluded that the EHTB method faithfully describes the main characteristics of the system. The use of a bigger basis set would merge the effective potential of the individual dots and mix up the array of quantum dots.

4. CONCLUSIONS

In this work it was investigated the electronic potentials that are obtained from parametrized tight-binding hamiltonians. From the fundamental viewpoint, it is desirable to guarantee that the underlying physics is preserved for a given choice of tight-binding parameters because several parameter sets can produce similar results, whereas, from the pragmatic viewpoint, it can also be said that the non-uniqueness of parametrization can be used to make numerical procedures as convenient as possible.

In this work the formalism was applied to the extended Hückel tight-binding (EHTB) hamiltonian, which consists of a two-center Slater-Koster method that makes explicit use of

the overlap matrix. The functional form of the effective electronic potential is determined by both the tight-binding parameters and the basis set states. In the case of molecular systems described by Slater-type orbitals the ensuing potential exhibits minima at the bond regions, as a result of the resonance integral (off-diagonal) matrix elements. The effective electronic potential $V_{eff}(\mathbf{r})$ tends to be shallower on the atomic sites. The effect is more pronounced as the principal quantum number of the STO basis set increases because only the valence orbitals are taken into account in the EHTB method. The effect is analogous to that produced by the use of pseudo-potentials in first-principle formalisms to avoid the ion potential on the core region. The electronic potential gained from the EHTB method also describes the effects produced by the different electronegativities of the atoms, giving rise to deeper bonding potentials for the more electronegative species. The method is also applied for the 2-(2'-hydroxyphenyl)benzothiazole (HBT) molecule, after optimization of the EHTB parameters to fit *ab-initio* calculations. The 2D potential profile is used to determine the polarity of the molecule.

As another application to the extended Hückel theory, that has been applied extensively to atomistic systems both in chemistry and physics, it was demonstrated a procedure to model arrays of quantum dots with the EHTB method in the basis of harmonic oscillator eigenstates. The approach is versatile and describes well the characteristics of the system.

5. ACKNOWLEDGMENTS

The author acknowledge financial support from Brazilian agencies FAPERJ, INCT – Carbon Nanomaterials, INCT – Materials Informatics and INCT – INEO for financial support. G.C. gratefully acknowledge FAPERJ, grant number E-26/200.627/2022 and E-26/210.391/2022 (project Jovem Pesquisador Fluminense process number 271814) for financial support. The authors also acknowledge the computational support of Núcleo Avançado de Computação de Alto Desempenho (NACAD/COPPE/UFRJ) and Sistema Nacional de Processamento de Alto Desempenho (SINAPAD).

Bibliography

- [1] L. Fu, C. L. Kane, E. J. Mele, Topological insulators in three dimensions, Phys. Rev. Lett. 98 (10) (2007) 106803. doi:10.1103/PhysRevLett.98.106803.
- [2] H. Eschrig, K. Koepnick, Tight-binding models for the iron-based superconductors, Phys. Rev. B 80 (10) (2009) 104503. doi:10.1103/PhysRevB.80.104503.
- [3] F. R. Renani, G. Kirczenow, Ligand-based transport resonances of single-molecule-magnet spin filters: Suppression of coulomb blockade and determination of easy-axis orientation, Phys. Rev. B 84 (18) (2011) 180408. doi:10.1103/PhysRevB.84.180408.
- [4] D. Kienle, J. I. Cerda, A. W. Ghosh, Extended hückel theory for band structure, chemistry, and transport. i. carbon nanotubes, J. Appl. Phys. 100 (4) (2006) 043714. doi:10.1063/1.2259818.
- [5] F. Mireles, G. Kirczenow, Ballistic spin-polarized transport and rashba spin precession in semiconductor nanowires, Phys. Rev. B 64 (2) (2001) 024426. doi:10.1103/PhysRevB.64.024426.
- [6] R. E. Cohen, M. J. Mehl, D. A. Papaconstantopoulos, Tight-binding total-energy method for transition and noble metals, Phys. Rev. B 50 (19) (1994) 14694. doi:10.1103/PhysRevB.50.14694.

- [7] J. Cerda, F. Soria, Accurate and transferable extended hückel-type tight-binding parameters, *Phys. Rev. B* 61 (12) (2000) 7965. doi:10.1103/PhysRevB.61.7965.
- [8] M. J. Mehl, D. A. Papaconstantopoulos, Applications of a tight-binding total-energy method for transition and noble metals: Elastic constants, vacancies, and surfaces of monatomic metals, *Phys. Rev. B* 54 (7) (1996) 4519. doi:10.1103/PhysRevB.54.4519.
- [9] H. Amara, J.-M. Roussel, C. Bichara, J.-P. Gaspard, F. Ducastelle, Tight-binding potential for atomistic simulations of carbon interacting with transition metals: Application to the ni-c system, *Phys. Rev. B* 79 (1) (2009) 014109. doi:10.1103/PhysRevB.79.014109.
- [10] F. R. Renani, G. Kirczenow, Tight-binding model of mn 12 single-molecule magnets: Electronic and magnetic structure and transport properties, *Phys. Rev. B* 85 (24) (2012) 245415. doi:10.1103/PhysRevB.85.245415.
- [11] A. Monti, C. F. A. Negre, V. S. Batista, L. G. C. Rego, H. J. M. de Groot, F. Buda, Crucial role of nuclear dynamics for electron injection in a dye-semiconductor complex, *J. Phys. Chem. Lett.* 6 (12) (2015) 2393–2398. doi:10.1021/acs.jpcclett.5b00876.
- [12] C. R. Medrano, M. B. Oviedo, C. G. Sánchez, Photoinduced charge-transfer dynamics simulations in noncovalently bonded molecular aggregates, *Phys. Chem. Chem. Phys.* 18 (22) (2016) 14840–14849. doi:10.1039/C6CP00231E.
- [13] J. C. Slater, G. F. Koster, Simplified lcao method for the periodic potential problem, *Phys. Rev.* 94 (6) (1954) 1498. doi:10.1103/PhysRev.94.1498.
- [14] W. M. C. Foulkes, R. Haydock, Tight-binding models and density-functional theory, *Phys. Rev. B* 39 (17) (1989) 12520. doi:10.1103/PhysRevB.39.12520.
- [15] T. A. Niehaus, S. Suhai, F. Della Sala, P. Lugli, M. Elstner, G. Seifert, T. Frauenheim, Tight-binding approach to time-dependent density-functional response theory, *Phys. Rev. B* 63 (8) (2001) 085108. doi:10.1103/PhysRevB.63.085108.
- [16] D. Porezag, T. Frauenheim, T. Köhler, G. Seifert, R. Kaschner, Construction of tight-binding-like potentials on the basis of density-functional theory: Application to carbon, *Phys. Rev. B* 51 (19) (1995) 12947. doi:10.1103/PhysRevB.51.12947.
- [17] S. Pal, D. J. Trivedi, A. V. Akimov, B. Aradi, T. Frauenheim, O. V. Prezhdo, Nonadiabatic molecular dynamics for thousand atom systems: a tight-binding approach toward pyxaid, *J. Chem. Theory Comput.* 12 (4) (2016) 1436–1448. doi:10.1021/acs.jctc.5b01231.
- [18] R. E. Cohen, L. Stixrude, E. Wasserman, Tight-binding computations of elastic anisotropy of fe, xe, and si under compression, *Phys. Rev. B* 56 (14) (1997) 8575. doi:10.1103/PhysRevB.56.8575.
- [19] M. S. Tang, C. Z. Wang, C. T. Chan, K. M. Ho, Environment-dependent tight-binding potential model, *Phys. Rev. B* 53 (1996) 979–982. doi:10.1103/PhysRevB.53.979.
- [20] R. Hoffmann, W. N. Lipscomb, Theory of Polyhedral Molecules. I. Physical Factorizations of the Secular Equation, *J. Chem. Phys.* 36 (8) (2004) 2179–2189. doi:10.1063/1.1732849.
- [21] W. Kohn, L. J. Sham, Self-consistent equations including exchange and correlation effects, *Phys. Rev.* 140 (1965) A1133–A1138. doi:10.1103/PhysRev.140.A1133.
- [22] J. P. Perdew, A. Zunger, Self-interaction correction to density-functional approximations for many-electron systems, *Phys. Rev. B* 23 (1981) 5048–5079. doi:10.1103/PhysRevB.23.5048. URL <https://link.aps.org/doi/10.1103/PhysRevB.23.5048>
- [23] J. Fernández Rico, R. López, G. Ramírez, Molecular integrals with Slater basis. I. General approach, *J. Chem. Phys.* 91 (7) (1989) 4204–4212. doi:10.1063/1.456799.
- [24] S. Alvarez, Tables of parameters for extended hückel calculations universitat de barcelona (2012).
- [25] W. E. Pickett, Pseudopotential methods in condensed matter applications, *Comput. Phys. Rep.* 9 (3) (1989) 115–197. doi:10.1016/0167-7977(89)90002-6.
- [26] R. L. Haupt, S. E. Haupt, *Practical genetic algorithms*, John Wiley & Sons, 2004. doi:10.1002/0471671746. URL <https://doi.org/10.1002/0471671746>
- [27] A. D. Becke, Density-functional thermochemistry. III. The role of exact exchange, *The Journal of Chemical Physics* 98 (7) (1993) 5648–5652. doi:10.1063/1.464913. URL <https://doi.org/10.1063/1.464913>
- [28] G. Candioto, R. Giro, B. A. C. Horta, F. P. Rosselli, M. de Cicco, C. A. Achete, M. Cremona, R. B. Capaz, Emission redshift in dcm2-doped alq₃ caused by nonlinear stark shifts and förster-mediated exciton diffusion, *Phys. Rev. B* 102 (2020) 235401. doi:10.1103/PhysRevB.102.235401.
- [29] R. Ditchfield, W. J. Hehre, J. A. Pople, Self-Consistent Molecular-Orbital Methods. IX. An Extended Gaussian-Type Basis for Molecular-Orbital Studies of Organic Molecules, *The Journal of Chemical Physics* 54 (2) (2003) 724–728. doi:10.1063/1.1674902. URL <https://doi.org/10.1063/1.1674902>
- [30] A. Nazir, B. W. Lovett, S. D. Barrett, J. H. Reina, G. A. D. Briggs, Anticrossings in förster coupled quantum dots, *Phys. Rev. B* 71 (2005) 045334. doi:10.1103/PhysRevB.71.045334.
- [31] P. V. Kamat, Quantum dot solar cells. semiconductor nanocrystals as light harvesters, *J. Phys. Chem. C* 112 (48) (2008) 18737–18753. doi:10.1021/jp806791s.
- [32] V. Popsueva, R. Nepstad, T. Birkeland, M. Førre, J. P. Hansen, E. Lindroth, E. Waltersson, Structure of lateral two-electron quantum dot molecules in electromagnetic fields, *Phys. Rev. B* 76 (2007) 035303. doi:10.1103/PhysRevB.76.035303.
- [33] C. R. Kagan, C. B. Murray, Charge transport in strongly coupled quantum dot solids, *Nat. Nanotechnol.* 10 (12) (2015) 1013–1026.
- [34] A. Adronov, J. M. J. Fréchet, Light-harvesting dendrimers, *Chem. Commun.* (2000) 1701–1710. doi:10.1039/B005993P.
- [35] J. Teyssandier, S. D. Feyter, K. S. Mali, Host-guest chemistry in two-dimensional supramolecular networks, *Chem. Commun.* 52 (2016) 11465–11487. doi:10.1039/C6CC05256H.
- [36] G. D. Scholes, G. R. Fleming, A. Olaya-Castro, R. Van Grondelle, Lessons from nature about solar light harvesting, *Nat. Chem.* 3 (10) (2011) 763–774. doi:10.1038/nchem.1145.
- [37] A. Hashemi, M. Hosseini-Farзад, A. Montakhab, Emergence of semi-localized anderson modes in a disordered photonic crystal as a result of overlap probability, *Eur. Phys. J. B* 77 (2010) 147–152. doi:10.1140/epjb/e2010-00250-y.
- [38] R. Hooverman, Anomalous nodes in the bound state wave functions for non-local potentials, *Nucl. Phys. A* 189 (1) (1972) 161–169. doi:https://doi.org/10.1016/0375-9474(72)90651-3.
- [39] M. Razavy, Quantum theory of tunneling, World Scientific, 2013.
- [40] E. K. Lenzi, B. F. de Oliveira, L. R. da Silva, L. R. Evangelista, Solutions for a schrödinger equation with a nonlocal term, *J. Math. Phys.* 49 (3) (2008) 032108. doi:10.1063/1.2842069.